CHEMISTRY
A EUROPEAN JOURNAL

DOI: 10.1002/chem.200501308

A Bridge between Pillared-Layer and Helical Structures: A Series of Three-Dimensional Pillared Coordination Polymers with Multiform Helical Chains

Dong-Rong Xiao,[a] En-Bo Wang,*[a] Hai-Yan An,[a] Yang-Guang Li,[a] Zhong-Min Su,*[b] and Chun-Yan Sun[a]

Abstract: Rational self-assembly of a long V-shaped 3,3′,4,4′-benzophenonetetracarboxylate (bptc) ligand and metal salts in the presence of linear bidentate ligand yield a series of novel pillared helical-layer complexes, namely, $[Cu_2(bptc)(bpy)_2]$ (**1**), $[M_3(Hbptc)_2(bpy)_3(H_2O)_4]\cdot 2H_2O$ (M = Fe(**2**) and Ni(**3**)), $[Co_2(bptc)(bpy)(H_2O)]\cdot 0.5\,bpy$ (**4**), $[Cd_2(bptc)(bpy)(H_2O)_2]\cdot H_2O$ (**5**), $[Mn_2(bptc)(bpy)_{1.5}(H_2O)_3]$ (**6**) and $[M_2(bptc)(bpy)_{0.5}(H_2O)_5]\cdot 0.5\,bpy$ (M = Mn(**7**), Mg(**8**) and Co(**9**), bpy = 4,4′-bipyridine). Their structures were determined by single-crystal X-ray diffraction analyses and further characterized by elemental analyses, IR spectra, and thermogravimetric (TG) analyses. The structure of **1** consists of two types of chiral layers, one left-handed and the other right-handed, which are connected by bpy pillars to generate a novel 3D open framework featuring four distinct helical chains. Compounds **2** and **3** are isostructural and feature 3D structures formed from the interconnection of arm-shaped helical layers with bpy pillars. Compound **4** is a pillared helical double-layer complex containing four different types of helices, among which the nine-fold interwoven helices constructed from triple-stranded helical motifs are unprecedented. Compound **5** exhibits a novel 3D covalent framework which features nanosized tubular channels. These channels are built from helical layers pillared by bptc ligands. The structure of **6** is constructed from $\{Mn(bptc)(H_2O)\}_n^{2n-}$ layers, which consist of left- and right-handed helical chains, pillared by $[Mn_2(bpy)_3(H_2O)_4]^{4+}$ complexes into a 3D framework. To the best of our knowledge, compounds **1**–**6** are the first examples of pillared helical-layer coordination polymers. Compounds **7**–**9** are isostructural and exhibit interesting 2D helical double-layer structures, which are constructed from $\{M(bptc)(H_2O)_2\}_n^{2n-}$ ribbons cross-linked by $[M_2(bpy)(H_2O)_6]^{4+}$ complexes. Furthermore, the 3D supramolecular structures of **7**–**9** are similar to the 3D structure of **6**, and the 2D structure of **7** can be transformed into the 3D structure of **6** at higher reaction temperature. By inspection of the structures of **1**–**9**, it is believed that the V-shaped bptc ligand and V-shaped phthalic group of the bptc ligand are important for the formation of the helical structures. The magnetic behavior of compounds **1**, **2**, **4**, **6**, and **9** was studied and indicated the existence of antiferromagnetic interactions. Moreover, compound **5** shows intense photoluminescence at room temperature.

Keywords: coordination polymers · helical structures · hydrothermal synthesis · pillared-layer structures · polymers

Introduction

The design and synthesis of porous metal–organic frameworks (MOFs), which provide pores of well-defined sizes, shapes, and chemical environments, are of great current interest; not only because of their tremendous potential applications in gas storage, chemical separations, ion exchange, microelectronics, nonlinear optics and heterogeneous catalysis, but also owing to their intriguing variety of architectures and topologies.[1–6] Consequently, a series of open metal–organic frameworks with various structural motifs, including honeycomb, brick wall, bilayer, ladder, herringbone, diamondoid, and rectangular grid, have been deliberately de-

[a] Dr. D.-R. Xiao, Prof. E.-B. Wang, Dr. H.-Y. An, Dr. Y.-G. Li, C.-Y. Sun
Institute of Polyoxometalate Chemistry
Department of Chemistry, Northeast Normal University
Changchun 130024 (China)
Fax: (+86) 431-509-8787
E-mail: wangenbo@public.cc.jl.cn

[b] Prof. Z.-M. Su
Institute of Functional Materials
Department of Chemistry, Northeast Normal University
Changchun, Jilin, 130024 (China)
E-mail: zmsu@nenu.edu.cn

Supporting information for this article is available on the WWW under http://www.chemeurj.org/ or from the author.

signed, and discussed in comprehensive reviews by Yaghi, Kitagawa, Rao, Chen and their co-workers.[7] Being an important subclass of porous materials, pillared-layer structures, which are frequently found in ancient buildings on the macroscopic scale, such as the Parthenon in Athens, have proved to be an effective and controllable route to design three-dimensional (3D) frameworks with large channels.[8–12] Employing this approach, a variety of pillared-layer structures including positively and negatively charged or neutral layers have been synthesized.[10] This research area soon became very attractive because of the merits of pillared-layer structures, such as control over the porous structures and the chemical functionality by simple modification of the pillar module.[12] These peculiar merits associated with the pillared-layer structures lead us to this interesting and challenging field.

Helical structures, which are ubiquitous in nature and are the foundation of the genetic code, have been attracting increased attention in coordination chemistry and materials chemistry due to their importance in biological systems, optical devices and asymmetric catalysis.[13–17] Many chemists have made great contributions to this field, and the design of helical coordination polymers through the self-assembly of ligands and metal cations has shown significant progress recently.[15,16] However, the occurrence of pillared-layer complexes with helical character is particularly rare. Having studied the literature, we noticed that although the helical layer motif (a layer containing helical chains, usually used in biology[14c]) was reported several years ago as a new two-dimensional motif,[17] studies on extending it into 3D open frameworks remained unexplored. Inspired by the aforementioned considerations, our current synthetic strategy is to acquire pillared porous MOFs with helical character by linking the helical layers with pillar modules of changeable length and/or type. Such a strategy should lead to new compounds combining respective merits of pillared-layer and helical structures.

In our strategy, 3,3′,4,4′-benzophenonetetracarboxylate (bptc) was chosen as the organic ligand based on the following considerations: i) although a few pillared structures are built upon carboxylate ligands,[18] exploitation for them to construct pillared 3D frameworks is still in its infancy and, therefore, further research is necessary to enrich and develop this field; ii) being an asymmetrically V-shaped ligand, it can induce a dissymmetric unit when coordinating with metal atoms, which may improve the helicity of polymeric chains and thus favor the formation of a helical structure;[13a,15a,17a] iii) by possessing three possible conformations (Scheme S1, Supporting Information) and multiple bridging moieties, a variety of connection modes with metal centers are possible and provide abundant structural motifs; therefore, bptc may be an excellent candidate for the construction of multidimensional coordination polymers, especially 3D open frameworks; iv) coordination polymers constructed from the bptc ligand have rarely been reported,[19] and much work is still necessary to understand the coordination chemistry of bptc.

Because of the low solubility of the ligands used and the resultant difficulty to grow crystals of coordination polymers, a hydrothermal technique was adopted in this paper to put the designed strategy into practice. A series of pillared coordination polymers were then synthesized successfully, namely $[Cu_2(bptc)(bpy)_2]$ (**1**), $[M_3(Hbptc)_2(bpy)_3(H_2O)_4]\cdot 2H_2O$ (M = Fe(**2**) and Ni(**3**)), $[Co_2(bptc)(bpy)(H_2O)]\cdot 0.5\,bpy$ (**4**), $[Cd_2(bptc)(bpy)(H_2O)_2]\cdot H_2O$ (**5**), $[Mn_2(bptc)(bpy)_{1.5}(H_2O)_3]$ (**6**) and $[M_2(bptc)(bpy)_{0.5}(H_2O)_5]\cdot 0.5\,bpy$ (M = Mn(**7**), Mg(**8**) and Co(**9**), bpy = 4,4′-bipyridine). The syntheses and crystal structures of these compounds are reported here. This work may provide a bridge between pillared-layer and helical systems.

Results and Discussion

Description of crystal structures: Single-crystal X-ray structural analysis shows that the structure of compound **1** is a pillared helical-layer complex containing four types of helices, in which the asymmetric unit contains one Cu atom, one bpy ligand and 0.5 bptc ligand (Figure 1). Each Cu^{II} atom is primarily coordinated by two oxygen atoms from two bptc ligands (Cu–O 1.960(5) and 1.966(5) Å) and two nitrogen atoms from two bpy ligands (Cu–N 2.033(6) and 2.057(7) Å) to furnish a distorted square-planar coordination. The remaining carboxylic oxygen atom has weak interaction with Cu1 at the axial site (Cu–O 2.716 Å) due to the Jahn-Teller effect. All the carboxylic groups of the bptc ligand adopt a monodentate mode to connect with four Cu atoms (Scheme S2a). Based on this connection mode, the Cu^{II} atoms are bridged by the V-shaped phthalic groups of bptc ligands to form the left- and right-handed helical chains running along a crystallographic 2_1 axis in the *c* direction with a pitch of 11.451 Å (Figure 2). As shown in Figure 2, adjacent same-handed helical chains are further intercon-

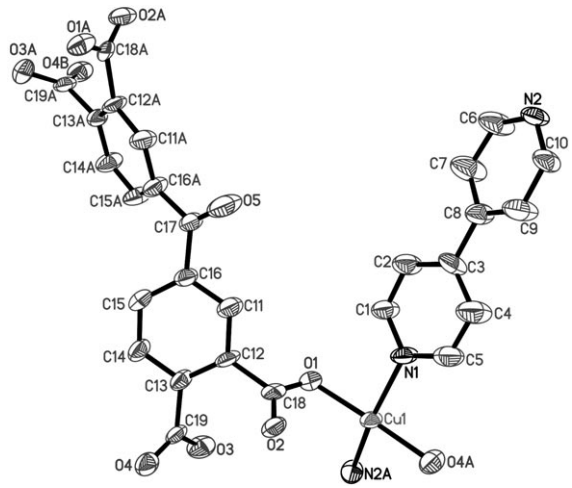

Figure 1. ORTEP drawing of **1** with thermal ellipsoids at 50% probability.

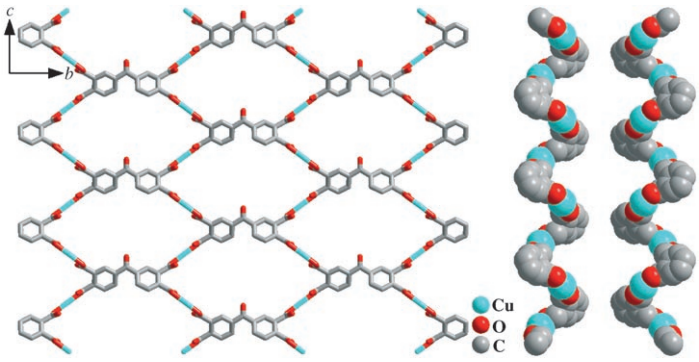

Figure 2. Left: Perspective view of the left-handed layer in **1**, showing rhombic windows with dimensions of 11.45×20.01 Å^2. Right: Space-filling diagram of the helical chains in the 2D helical layers.

nected by carbonyl groups of bptc to generate a 2D chiral layer of very large rhombic windows (with dimensions of 11.45×20.01 Å). Interestingly, the two types of chiral layers, one left-handed and the other right-handed (Figure S1a), are connected by bpy pillars to generate a novel 3D open framework (Figure 3a) featuring asymmetric cavities with dimensions of 14.43×11.45×7.98 Å (Figure S1c). From the topological point of view, this 3D network can be regarded as a uninodal four-connected net with ($6^5$8) topology (Figure 3b), in which the Cu atoms act as four-connecting nodes. To our knowledge, this four-connected net is completely new within coordination polymer chemistry and the finding of this new topology is useful at the basic level in the crystal engineering of coordination networks. The Schläfli notation of this net, as we can see, is different but closely related to that of diamond (6^6) (Figure S2).[22]

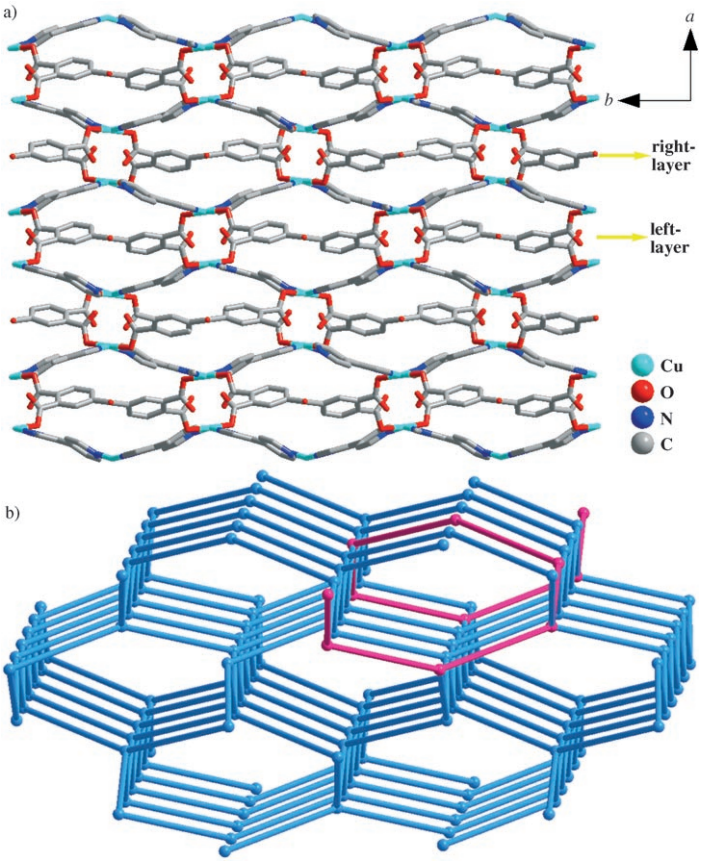

Figure 3. a) 3D network of **1** viewed along the *b* axis. b) Schematic illustrating the ($6^5$8) topology of the 3D network of **1**. One strand of a quadruple helix is highlighted (red).

The most fascinating structural feature of **1** is that the four distinct helical chains running along the crystallographic *c* axis coexist in the 3D network. This case is rather rare even though a few elegant coordination networks containing two types of helices have previously been characterized.[16,17a] Besides the single-helical chains in the 2D helical layer, there are a quadruple-stranded helix with a period of 45.804 Å (Figure 4a), and two types of double-stranded helices with a pitch of 22.902 Å (Figure 4b and c) in **1**. As depicted in Figure 4a, the quadruple-stranded helices are built from V-shaped O_2C-C-C-CO_2 groups and bpy ligands bridged between the Cu centers. Compared with a few precedents of double- and triple-stranded helical motifs,[13,15] the unusual intertwined quadruple-stranded helix is particularly rare in metal–organic complexes. Noteworthy of mentioning here is that the helical tube formed by the quadruple-stranded helices is separated by benzophenone groups of bptc (Figure S1b) to form the asymmetric cavities mentioned above. Whereas asymmetric cavities are particularly desirable because of their promising applications in asymmetric catalysis and chiral separations, such cavities enclosed by intertwined quadruple-stranded helices are extremely rare. The first type of double-stranded helix (Figure 4b) is also constructed by O_2C-C-C-CO_2 groups and bpy ligands bridged between the Cu centers. However, the helical tube formed by this helix is larger than that observed in the quadruple-stranded helix, whereas the second type of double-stranded helix is formed by bptc and bpy bridging the Cu atoms (Figure 4c).

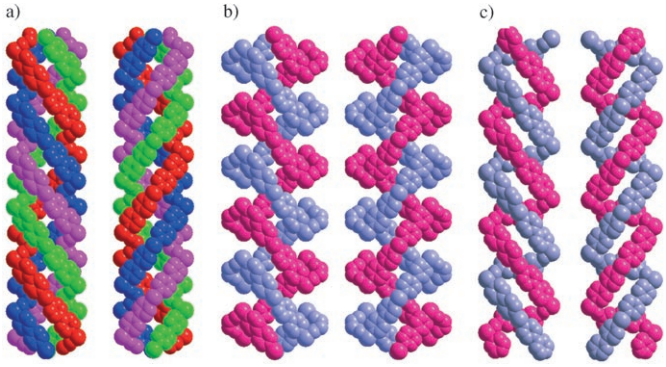

Figure 4. Space-filling views of the a) quadruple-stranded helices, b) the first type of double-stranded helix, and c) the second type of double-stranded helix in **1**.

When Fe and Ni, two transition metals with octahedral geometry, were used instead of Cu, structurally different 3D

frameworks are formed in **2** and **3** under similar reaction conditions. Compounds **2** and **3** are isostructural, so only the structure of **2** will be discussed herein. There are three crystallographically independent Fe centers in the asymmetric unit of **2** (Figure 5). They all exhibit distorted octahedral geometries. The Fe1 and Fe2 centers have identical coordination environments, both coordinated by two carboxylate oxygen atoms (Fe1–O3 2×2.118(3) Å, Fe2–O1 2×2.093(3) Å) from two different bptc ligands, two nitrogen atoms (Fe1–N1 2×2.153(3) Å, Fe2–N2 2.224(4) Å, Fe2–N3 2.177(4) Å) from two bpy ligands, and two coordinated water molecules (Fe1–OW1 2×2.122(3) Å, Fe2–OW2 2×2.142(3) Å). The Fe3 center is defined by four carboxylate oxygen atoms (Fe3–O2 2×2.150(3) Å, Fe3–O4 2×2.085(3) Å) of two different bptc ligands and two nitrogen atoms (Fe3–N4 2.197(4) Å, Fe3–N5 2.206(4) Å) of two bpy ligands. Unlike those in compound **1**, only one end of the carboxylic groups of the bptc ligand take part in the coordination with metal atoms, while the other end of the carboxylic groups act as the hydrogen-bond acceptors to link with the adjacent layers (Scheme S2b). In addition, the conformation of bptc in **2** is also different from that in **1**.

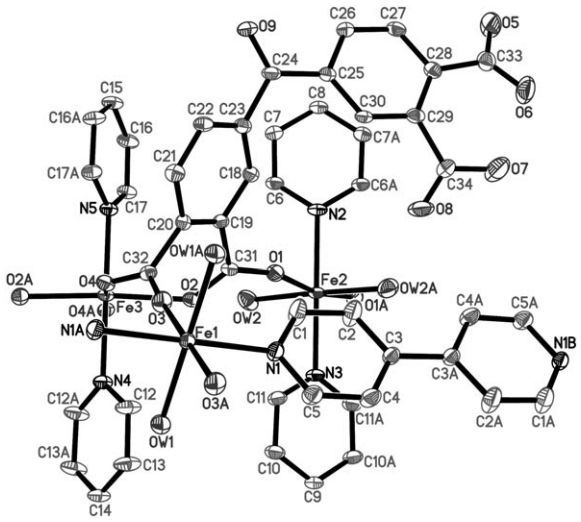

Figure 5. ORTEP diagram showing the coordination environments for the Fe atoms in **2**.

As shown in Figure 6a, the adjacent Fe2 and Fe3 atoms are linked by the carboxylic groups of bptc to form Fe-O-C-O-Fe helical chains (Fe···Fe 5.705(1) Å) running along the crystallographic *a* axis with a pitch of 11.370 Å (Figure 6b); the neighboring Fe1 and Fe3 atoms are also bridged by the carboxylic group of bptc to generate Fe-O-C-O-Fe chains running along the *c* axis with the Fe···Fe distance 6.026(1) Å. The two types of chains share Fe3 atoms, and give rise to a 2D sheet in which adjacent Fe1 atoms are further connected by bpy into the third type of Fe-bpy-Fe chain. Besides the helical chains running along *a* axis, there is another type of helix (Figure 6b) formed by carboxylic groups and V-shaped O_2C-C-C-CO_2 groups bridging between the Fe centers along the [101] direction with a pitch of 24.893 Å in the 2D layer. Interestingly, the one-end coordinated bptc ligands, grafted on the 2D sheet, are just like open arms protruding from the both sides of the sheet (Figure S4a).[3b,19,23b] As far as we know, such arm-shaped layers with helical characters is still very rare in systems of metal–organic complexes. As can be seen from Figure 7, adjacent helical layers are linked by bpy ligands as molecular pillars to form a novel 3D framework (Figure S4b) with parallelogrammic tubular channels (12.05×11.49 Å); the one-end coordinated bptc ligands and free water molecule reside in the channels. From a topological perspective, the structure of **2** can be simplified to a unique (4,6)-connected net with $(4^4 6^2)(4^8 6^7)$ topology. In this simplification the four-connecting nodes are the Fe1 centers and the six-connecting ones are the Fe3 centers (see Figure 7).

Interestingly, when the hydrothermal reactions of bptc, bpy and metal salts were carried out at about pH 9.0, compounds **4**–**6** with different structures were obtained. Compound **4** is a pillared helical-double-layer complex containing four types of helices. There are two crystallographically independent Co atoms in this structure (Figure 8). The Co1 atom is coordinated by one nitrogen atom from a bpy ligand, and three bridging oxygen atoms from three differ-

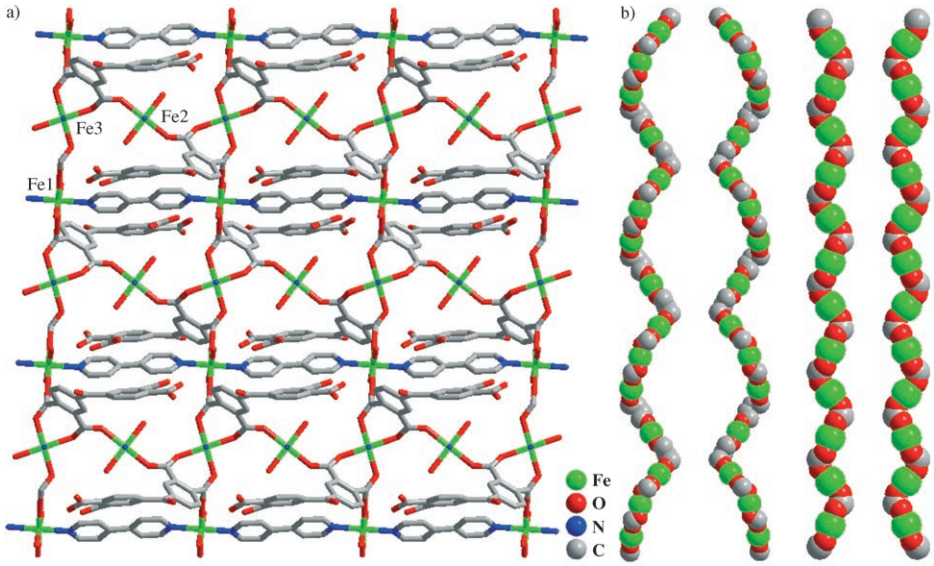

Figure 6. a) 2D helical layer in **2** viewed along the *b* axis. b) Space-filling views of two types of helices in the helical layer of **2**.

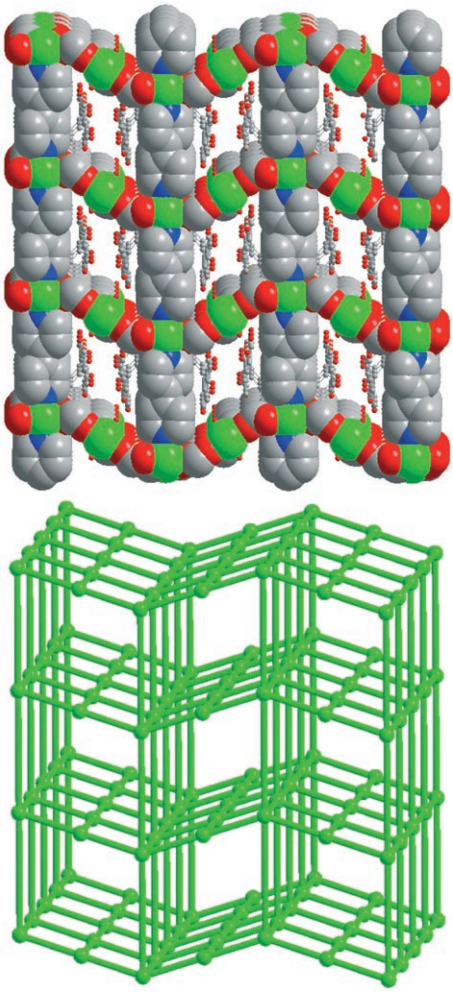

Figure 7. Top: Space-filling view of the 3D structure of **2** along the *a* axis, showing the parallelogrammic tubular channels occupied by one-end coordinated bptc ligands. Bottom: A schematic representation of the (4,6)-connected net of $(4^4 6^2)(4^8 6^7)$ topology.

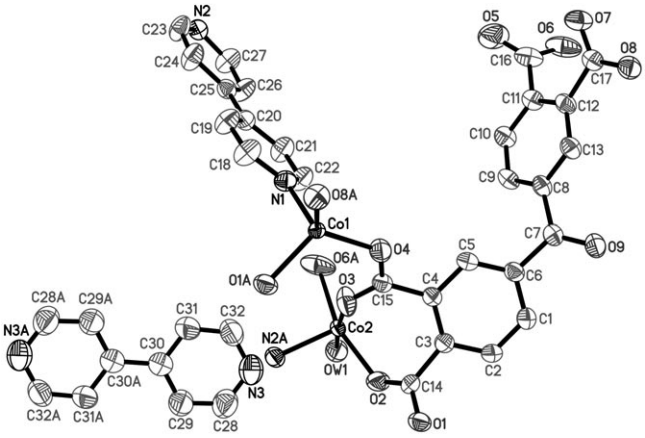

Figure 8. ORTEP drawing of **4** with thermal ellipsoids at 50% probability.

ent bptc ligands, to yield a distorted tetrahedral geometry. The Co2 center is coordinated in a distorted square pyramidal geometry to three carboxylate oxygen atoms from two bptc ligands, to one nitrogen atom of a bpy ligand, and to one aqua ligand.[24] The four carboxylic groups of the bptc ligand exhibit two kinds of coordination modes with the Co atoms, as shown in Scheme S2c. That is, two of them adopt a bidentate mode, while the other two exhibit a monodentate mode. Based on these connection modes, four Co^{II} ions are bridged by two pairs of bptc μ-carboxylate ends to give tetranuclear units that are further extended by bptc bridging ligands into 2D double layers (Figure 9a and Figure S5a). As shown in Figure 9b, the Co1 and Co2 atoms are linked by carboxylic groups and O_2C-C-C-CO_2 groups of bptc ligands to form the left- and right-handed helical chains running along a crystallographic 2_1 axis in the *b* direction with a pitch of 14.993 Å. To the best of our knowledge, such a double layer containing helices has not been reported in the system of metal carboxylates. Interestingly, adjacent helical double layers are connected by bpy pillars to generate a novel 3D open framework featuring large cavities with dimensions of $12.59 \times 7.01 \times 11.00$ Å^3, which are populated by the uncoordinated bpy molecules (Figure 9c and S5b). As shown in Figure 9d, these cavities are connected to each other via a small window of approximately 4.0 Å to from a 1D zigzag channel along the [100] direction (Figure S5d).[22a] Such a 3D open framework can also be viewed as a unique molecular "double-floor", directly linked by pillars through covalent bonds (Figure 10a and S5c). As far as we know, few examples of pillared double-layer structures have been reported previously.[14e] More interestingly, if the $[Co_4(CO_2)_4]$ tetranuclear unit is regarded as an eight-connecting node (Figure S6), the structure of **4** can be simplified as an eight-connected net with CsCl $(4^{24}6^4)$ topology (Figure 10b).[23]

Similar to **1**, four different types of helical chains running along the *b* axis in the 3D framework of **4** also exist. Apart from the single helical chains in the 2D helical double layer, there are two types of triple-stranded helices with a pitch of 44.979 Å (Figure 11a and c) and another single-stranded helix formed by bpy bridges between the Co centers with a pitch of 14.993 Å (Figure 11d) in **4**. As depicted in Figure 11a, the first type of triple-stranded helix is built from bptc and bpy bridge between the Co centers, and each triple-stranded helix is entangled by two neighboring triple-stranded helices to give an unprecedented nine-fold interwoven helix (Figure 11b). The second type of triple-stranded helix (Figure 11c) is also constructed by bptc and bpy bridged between the Co centers. However, the helical tube formed by this type of triple-stranded helix is smaller than that observed in the former.

Compound **5** exhibits a novel 3D covalent framework featuring nanosized tubular channels that are built from helical layers pillared by bptc ligands. There are two unique Cd atoms in the asymmetric unit of **5** (Figure 12). The Cd1 atom is coordinated by one nitrogen atom from a bpy ligand, three oxygen atoms from two carboxylic groups of two bptc ligands, and two aqua ligands, and shows a distorted octahedral geometry. The Cd2 atom is seven-coordinated by three pairs of chelating oxygen atoms from three differ-

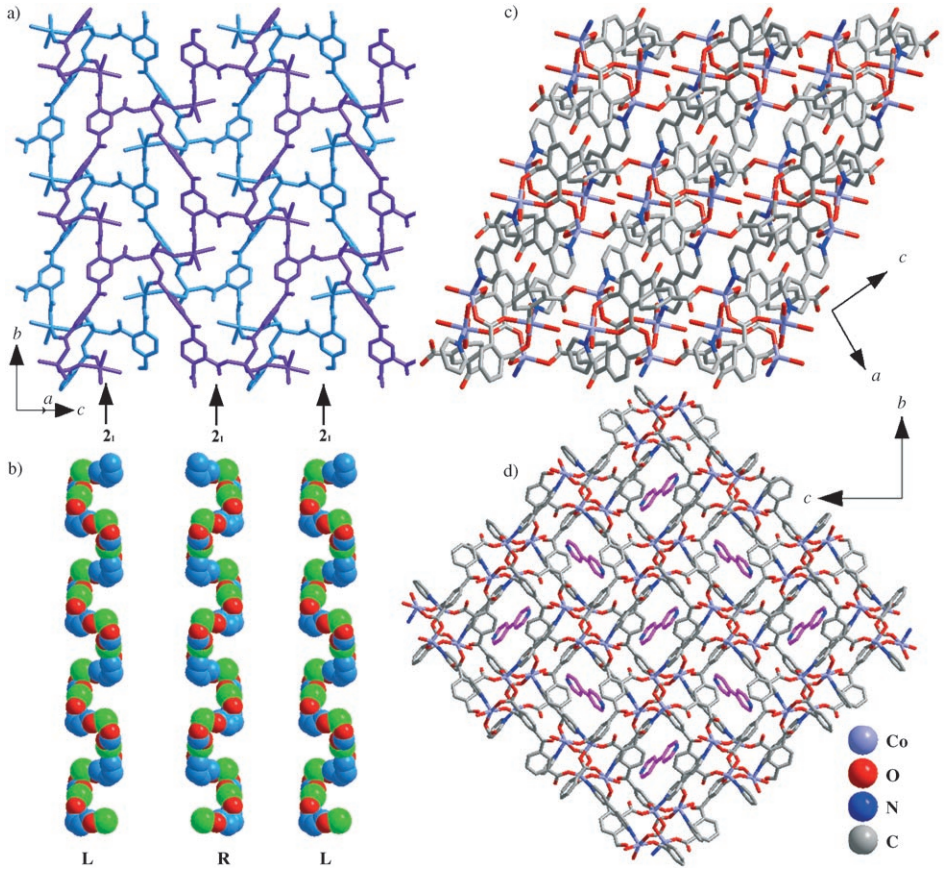

Figure 9. a) View of the 2D helical double layer in **4**. b) Space-filling diagram of the helical chains in the 2D helical double layer. c) 3D network of **4** viewed along the *b* axis. d) Perspective view of the 3D network in **4**, highlighting the zigzag channels occupied by the uncoordinated bpy molecules.

ent bptc ligands, and a bridging oxygen atom from the fourth bptc ligand. Its coordination geometry can be described as a distorted pentagonal bipyramid. Unlike in compounds **1**–**4**, the bptc ligand in **5** acts as a decadentate ligand; two carboxylic groups adopt a bidentate chelating mode, while the other two exhibit a tridentate chelating/bridging mode (Scheme S2d).

A striking feature of **5** is the alternating arrangement of two types of helices along the *b* axis to form a 2D chiral layer (Figure 13a and Figure S7). One helix is formed by carboxylic oxygen atoms bridging Cd atoms, which is generated around the crystallographic 2_1 axis with a pitch of 13.699 Å (Figure 13b). As far as we know, such an inorganic helix is still very rare in metal–organic complexes.[17a] The other type of helix is built from V-shaped O_2C-C-C-CO_2 bridges between the Cd centers with a pitch of 13.699 Å (Figure 13b), displaying an opposite helical orientation to the former helix. As shown in Figure 13a, the one-end coordinated bpy groups, grafted on the 2D chiral layer, are just like open arms (with length of ca. 9.3 Å) protruding from the both sides of the sheet (Figure S8).[3b,19,23b] To the best of our knowledge no chiral arm-shaped layers have been documented to date. Moreover, a careful examination shows that the inorganic helices in layer A (Figure 13c) are exclusively right-handed, whereas those in the neighboring layer B are exclusively left-handed (Figure S9). In other words, the helices in adjacent layers A and B are pairs of enantiomers, thus leading to a mesomeric network. More interestingly, adjacent chiral layers are pillared by bptc ligands to form a 3D microporous framework (Figure 13c) with nanosized tubular channels (17.33 × 12.26 Å). The monodentate bpy ligands and free water molecules reside in the channels. The bpy molecules, acting as ancillary ligands, are labile[20] and can be removed at 350 °C to form a stable phase formulated as $[Cd_2(bptc)]$ (Figure 13d), as confirmed by the TG analysis and elemental analysis. The TG curve of **5** (Figure S26) exhibits two weight-loss stages in the temperature ranges 135–240 (6.79 %) and 265–350 °C (19.43 %), corresponding to the release of water molecules and bpy groups, respectively. According to the TG analysis, **5** was heated in air at 350 °C for 12 h to remove the bpy ligands and water molecules (defined as **5a**). Elemental analysis of **5a** (C 35.47, H 1.16, Cd 38.61 %) agrees well with the expected formula for the opened $[Cd_2(bptc)]$ network (calcd: C 35.26, H 1.04, Cd 38.83 %).

X-ray crystallographic analysis reveals that the structure of **6** is constructed from $\{Mn(bptc)(H_2O)\}_n^{2n-}$ layers, which consist of left- and right-handed helical chains pillared by $[Mn_2(bpy)_3(H_2O)_4]^{4+}$ complexes into a 3D framework. The fundamental unit of **6** is shown in Figure 14. There are two crystallographically independent Mn centers, each displaying a distorted octahedral coordination geometry. The Mn1 center is coordinated by two carboxylate oxygen atoms of a bptc ligand, two nitrogen atoms of two bpy ligands, and two aqua ligands. The Mn2 center is defined by five carboxylate oxygen atoms of four different bptc ligands and one aqua ligand. Unlike in compounds **1**–**5**, the bptc ligand in **6** acts as a heptadentate ligand; three carboxylic groups adopt a bidentate mode, while the other one exhibits a monodentate mode (Scheme S2e). On the basis of this connection mode, all Mn1 centers are linked by four bridging bptc ligands to form a 2D layer lying the $(1\bar{1}0)$ plane (see Figure 15a). As depicted in Figure 15b, the Mn1 atoms are bridged by the V-shaped bptc ligands to form the left- and right-handed helices running along the *c* axis with a pitch of 13.880 Å. Of par-

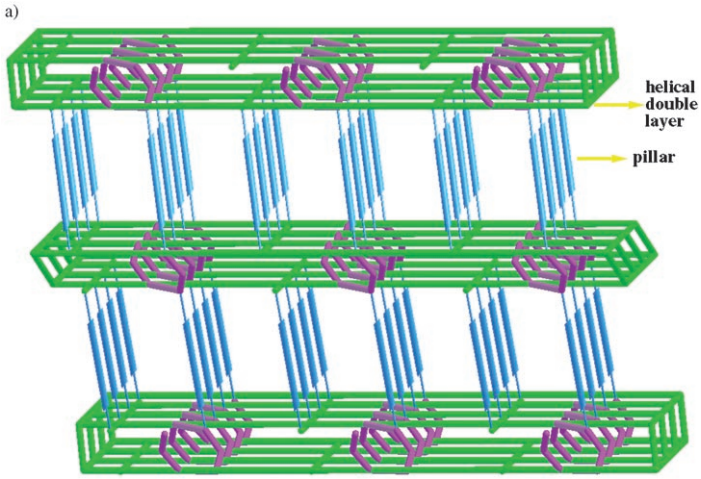

Figure 10. a) Schematic illustration of the pillared helical-double-layer structure of **4**. b) Schematic view of the CsCl ($4^{24}6^4$) topology of **4**.

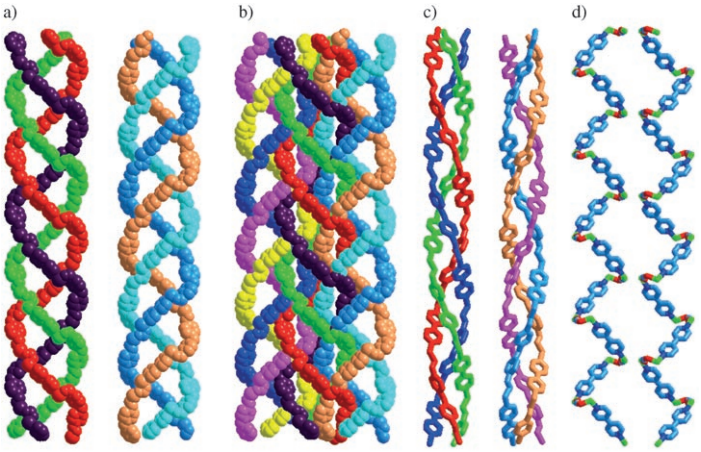

Figure 11. Space-filling views of the first type of a) triple-stranded helices and b) nine-fold interwoven helices in **4**. Perspective views of the second type of c) triple-stranded helices and d) single-stranded helices in **4**.

ticular interest is that adjacent helical layers are connected by $[Mn_2(bpy)_3(H_2O)_4]^{4+}$ complexes as molecular pillars to form a novel 3D framework featuring large channels along

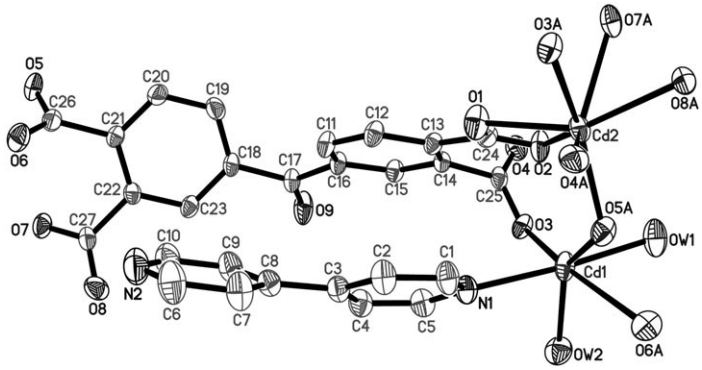

Figure 12. ORTEP drawing of **5** with thermal ellipsoids at 50% probability. The lattice water molecule has been omitted for clarity.

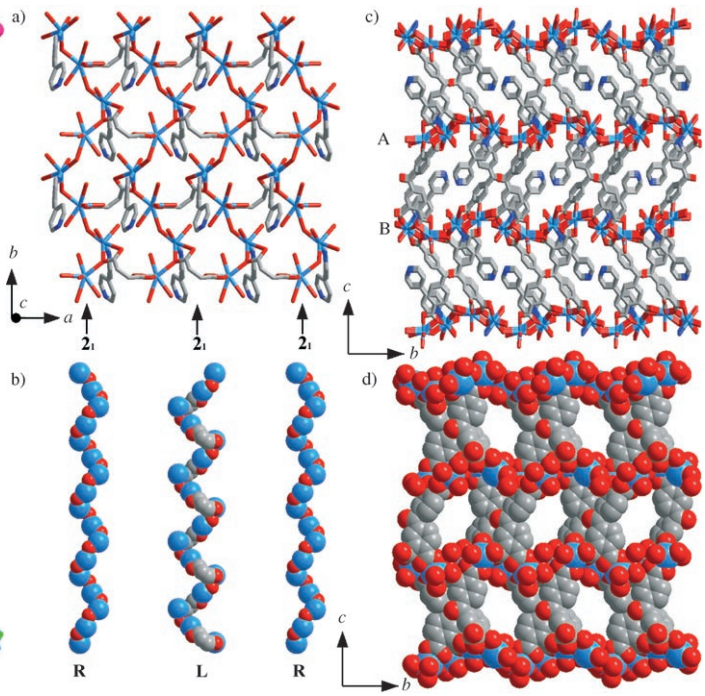

Figure 13. a) Perspective view of the chiral arm-shaped layers in **5**. b) Space-filling views of two types of helices in the chiral layer. c) 3D network of **5** viewed along the *a* axis. d) Space-filling view of **5** (bpy and water molecules are omitted for clarity).

the [001] direction occupied by the monodentate bpy ligands (Figure 16). So far, the examples of pillared coordination polymer involving metal–organic complexes as pillars are still very rare. As illustrated in Figure 17, the 3D network of **6** also contains elliptically shaped channels running along the *a* axis (Figure S11).

When the reaction time was reduced to 72 h and the reaction temperature was decreased to 110 °C, compounds **7**, **8** and **9** with layered structures were isolated. Compounds **7**–**9** are isostructural and the structure of **7** will be discussed in detail as a representative example. The asymmetric unit of **7** has two crystallographically independent Mn atoms; both

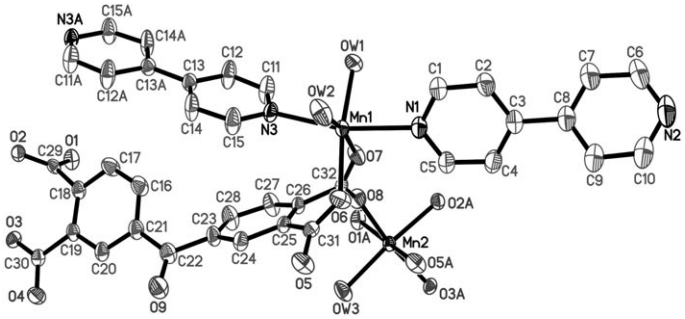

Figure 14. ORTEP drawing of **6** with thermal ellipsoids at 50% probability.

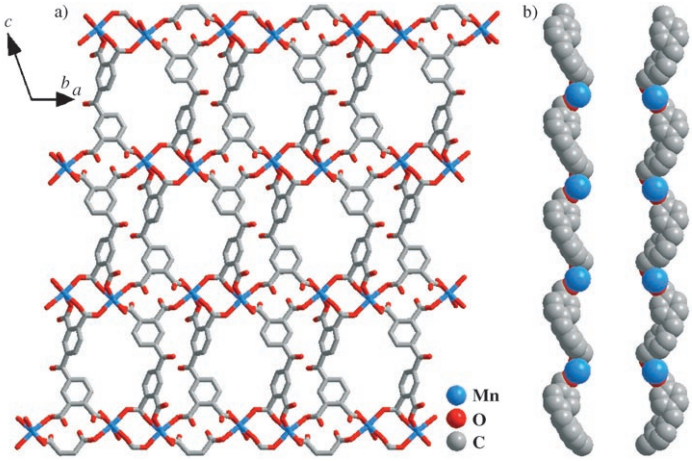

Figure 15. a) 2D helical layer in **6** viewed along [1$\bar{1}$0] direction. b) Space-filling diagram of the helical chains in the 2D helical layer.

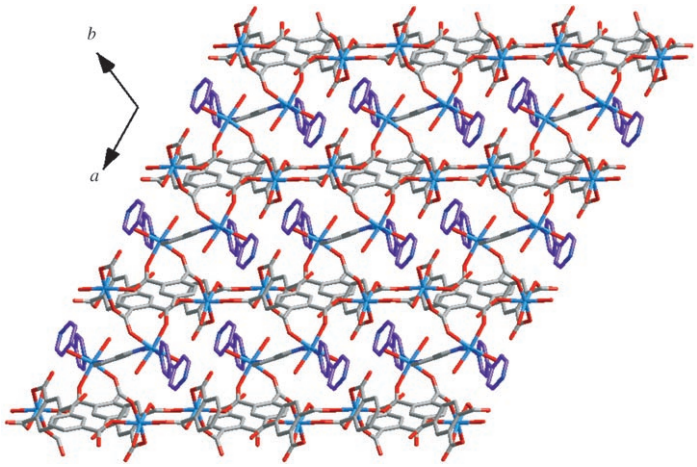

Figure 16. Perspective view of the 3D structure of **6** along the *c* axis, highlighting the channels occupied by one-end coordinated bpy ligands.

exhibit distorted octahedral geometries (Figure 18). Mn1 is coordinated by two carboxylate oxygen atoms, one nitrogen atoms, and three aqua ligands; Mn2 is ligated to four different carboxylate oxygen atoms and two aqua ligands. Differ-

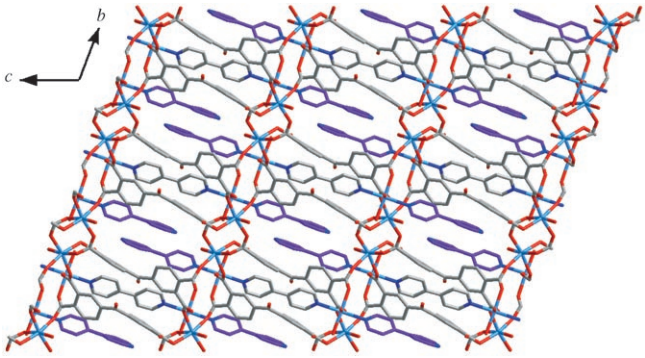

Figure 17. Perspective view of the 3D structure of **6** along the *a* axis, highlighting the elliptic-shaped channels occupied by one-end coordinated bpy ligands.

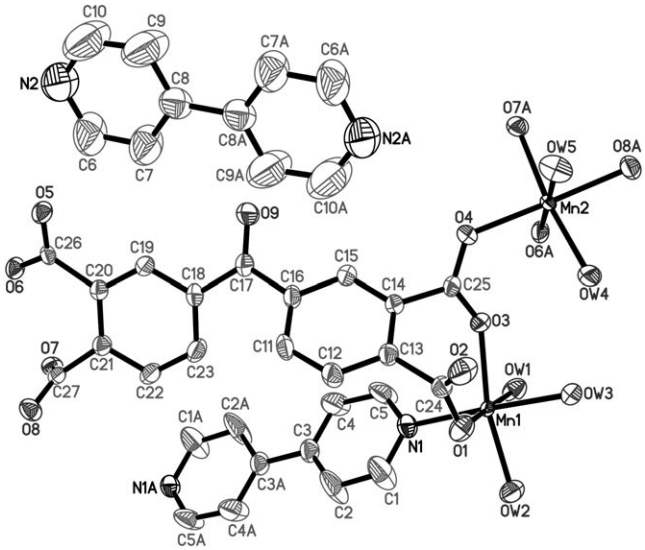

Figure 18. ORTEP drawing of **7** with thermal ellipsoids at 50% probability.

ent from that in compounds **1**–**6**, the bptc ligand in **7** adopts a hexadentate bridging coordination mode; two carboxylic groups bridge four Mn^{II} ions bidentately, and the other two adopt a monodentate coordination mode and connect with two metal ions (Scheme S2f). As shown in Figure S14, two Mn2 centers are bridged by a pair of bptc μ-carboxylate ends into a dimer unit. Neighboring dimer units are further linked by bptc ligands alternatively along two different directions to form a double-chain-like ribbon (Figure S14). The most interesting structural feature of **7** is that the adjacent $\{Mn(bptc)(H_2O)_2\}_n^{2n-}$ ribbons are covalently connected by the $[Mn_2(bpy)(H_2O)_6]^{4+}$ complex moieties to form a 2D sheet (Figure 19). Interestingly, the Mn atoms distributed in the sheet are not coplanar. Rather, half fall in one plane and half in an adjacent plane, resulting in the generation of a distinct 2D double-layer architecture with a distance of 4.8 Å between the two single layers (Figure S15). It is noteworthy that the double layer consists of left- and right-

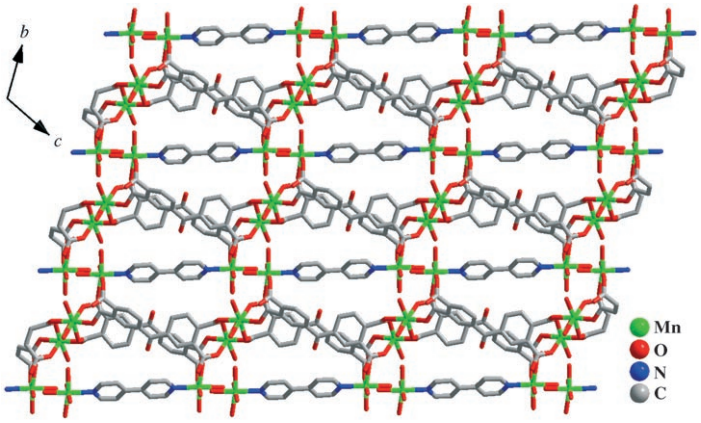

Figure 19. 2D double layer in **7** viewed along the *a* axis.

handed helices, which are constructed by bptc and bpy bridged between the Mn centers along the *b* axis with a pitch of 10.819 Å (Figure S16). These helical double layers are further connected by means of OW−H···O hydrogen bonds (OW5···O2 2.793 Å, OW2···O2 2.786 Å and OW3···O1 2.768 Å) to generate a 3D supramolecular network featuring large cavities with dimensions of $9.96\times10.81\times11.39$ Å^3

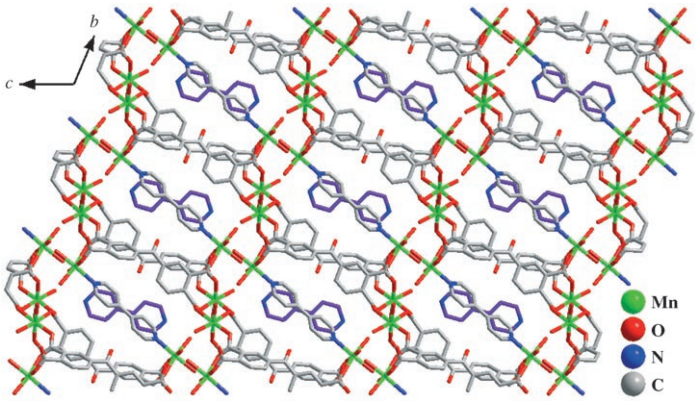

Figure 20. 3D supramolecular network of **7** viewed along the *a* axis, highlighting the uncoordinated bpy molecules occupying the cavities.

(Figure 20). As shown in Figures 21, 22 and Figure S18, these cavities are connected to each other by small windows to form multidirectional intersecting zigzag channels.[22a] Free bpy molecules are located in the channels and form multipoint hydrogen bonds with coordinated water molecules and carboxylate oxygen atoms (OW4···N2 2.827 Å and C6···O5 3.353 Å).

Strikingly, when viewed along the [111] direction, the 3D supramolecular structure of **7** (Figure 21) is similar to the 3D structure of **6** (Figure S21). Therefore, the 3D structure of **7** can also be considered as being constructed from 2D hydrogen-bonded layers (Figure S19a), which consist of $\{Mn(bptc)(H_2O)_2\}_n^{2n-}$ ribbons, pillared by $[Mn_2(bpy)(H_2O)_6]^{4+}$ complexes. Furthermore, a careful comparison of

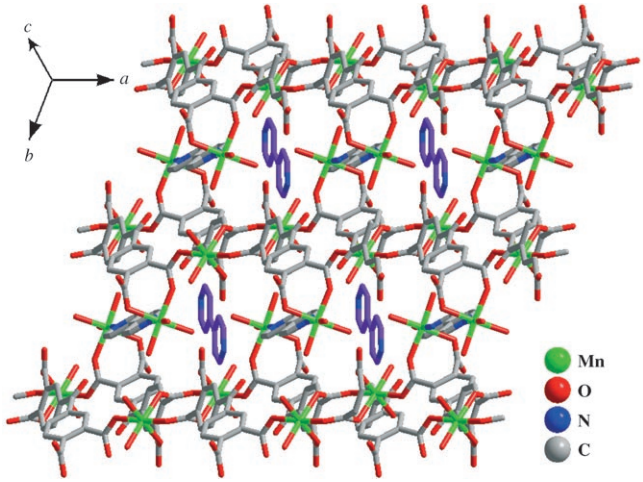

Figure 21. Perspective view of the 3D supramolecular network in **7**, highlighting the zigzag channels along the [111] direction.

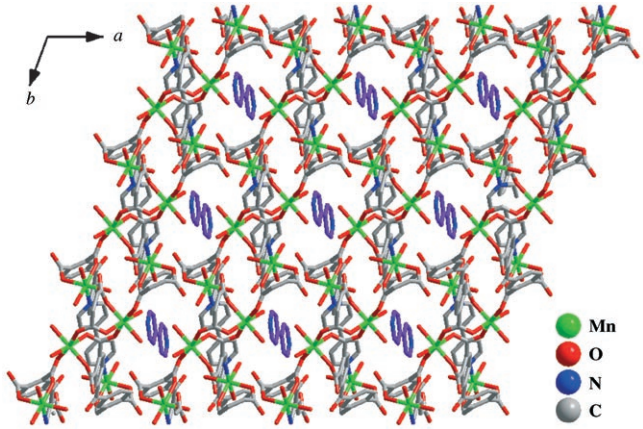

Figure 22. Perspective view of the 3D supramolecular network in **7**, highlighting the zigzag channels along the *c* axis.

7 with **6** shows that the $\{Mn(bptc)(H_2O)_2\}_n^{2n-}$ hydrogen-bonded layer can be converted into the $\{Mn(bptc)(H_2O)\}_n^{2n-}$ layers in **6** by the replacement of the aqua ligands (OW5) by carboxylate oxygens (O2) (Figure S19 and Figure S20). The $[Mn_2(bpy)(H_2O)_6]^{4+}$ pillars in **7** can also be converted into the $[Mn_2(bpy)_3(H_2O)_4]^{4+}$ pillars in **6** by the replacement of the aqua ligands (OW3) by free bpy ligands (Figure S21). This comparison may suggest the possible transformation of **7** into **6** through the replacement of aqua ligands by carboxylate oxygen atoms and bpy.[21b,c] So far, we have not achieved the chemical interconversion between **6** and **7**. However, compound **6** can be prepared by a modification in the reaction used to synthesize **7**.

In a comparison of the structures of **1**–**9**, it was found that coordination modes and conformations of the bptc ligand and coordination geometry of the central metal ion may have a very significant effect on the final structure. As demonstrated by the comparison of compounds **1** and **5** with **6**–**9**, the change in coordination geometry of the central metal

ion causes the distinctness of the linking fashion of the subunits and finally results in the formation of different structures, even though the conformation of the bptc ligand is the same. In addition, the steric conformation of the bptc ligand also plays a crucial role in the formation of the resulting structure, as evidenced by the comparison of compounds **2** and **3** with **6**–**9**. Due to the conformation of bptc in **2** and **3** being different from that in **6**–**9**, the coordination modes of bptc are obviously different (Scheme S2), which may thus lead to the formation of different structures in **2** and **3** and **6**–**9**. Furthermore, by inspection of the structures of **1**–**9**, it is believed that the V-shaped bptc ligand and the V-shaped phthalic group of the bptc ligand are important for the formation of the helical structures, which further confirms that the employment of V-shaped organic bridges could improve the helicity of polymeric chains.[13a,15a]

It should also be noted that the other structure-influencing factors, such as pH value and reaction temperature, could affect the overall structure obtained.[21] Due to the existence of protonated and/or deprotonated carboxyl groups, the bptc ligand can exist in protonated and partially and/or fully deprotonated forms in solution, depending on the pH. Furthermore, the connecting pattern of the bptc ligand also depends on the pH. In a comparison of compounds **1**–**3** with **4**–**9**, it was found that the increase in pH resulted in a higher connectivity level of bptc ligands, which in turn affects the formation of the final structure. In addition, the comparison of compound **6** with **7** also shows that reaction temperature may play a key role in determining the dimension of the resulting structure. At higher reaction temperatures, part of the aqua ligands was replaced by carboxylate oxygens and bpy, which is a critical factor for the transformation of a 2D structure in **7** into a 3D structure in **6**.[21b]

Photoluminescence properties: Taking the excellent luminescent properties of polynuclear d^{10} metal complexes into account, the luminescence of **5** was investigated. Compound **5** exhibits an intense emission maximum at $\lambda = 514$ nm upon excitation at $\lambda = 368$ nm (Figure 23). In order to understand the nature of the emission band, the photoluminescence properties of the H_4bptc ligand was analyzed. It was found that a weakly similar emission ($\lambda_{max} = 520$ nm) could be observed for the free H_4bptc ligand (Figure S22). Therefore, the emission of **5** may be assigned to intraligand fluorescent emission. The enhancement of luminescence may be attributed to ligand chelation to the metal center, which effectively increases the rigidity and asymmetry of the ligand and reduces the loss of energy by radiationless decay. This observation indicates that compound **5** may be an excellent candidate for potential photoactive materials, since this condensed material is thermally stable and insoluble in common polar and nonpolar solvents.

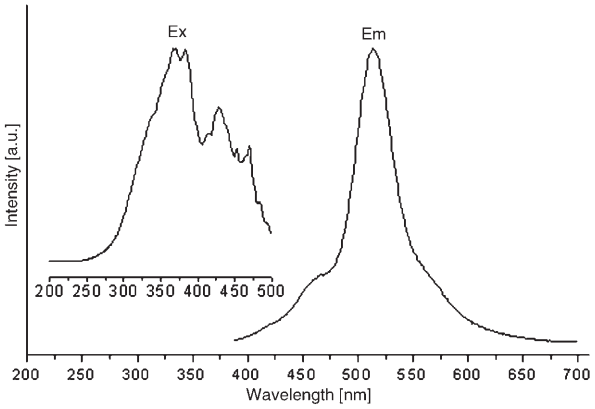

Figure 23. Solid-state emission spectra of compound **5** at room temperature.

Magnetic properties: The magnetic properties of **1**, **2**, **4**, **6**, and **9** were investigated over the temperature range 2.0–300.0 K (Figure 24). For **1**, the $\chi_M T$ value at 300 K is 1.232 $cm^3 K mol^{-1}$ (3.139 μ_B), which is much higher than the expected value (0.750 $cm^3 K mol^{-1}$, 2.449 μ_B) of two isolated spin-only Cu^{II} ions ($S = {}^1/_2$, $g = 2.0$; Figure 24a). As T is lowered, $\chi_M T$ decreases continuously to a value of 0.355 $cm^3 K mol^{-1}$ at 2 K. This behavior indicates a dominant antiferromagnetic interaction between the Cu^{II} ions in the structures. As the shortest Cu···Cu distance across the bpy bridge is 11.204 Å in **1**, the magnetic exchange coupling through the bpy bridge is expected to be very weak.[25] The observed antiferromagnetic interaction, therefore, should mainly arise from the magnetic superexchange through the O_2C-C-C-CO_2 bridge. The $1/\chi_M$ versus T plot of **1** is in correspondence with the Curie–Weiss law in the range of 16–300 K, with $C = 1.255$ $cm^3 K mol^{-1}$ and $\theta = -14.000$ K.

For **2**, the $\chi_M T$ value at 300 K is 11.564 $cm^3 K mol^{-1}$ (9.618 μ_B), which is higher than the expected value (9.000 $cm^3 K mol^{-1}$, 8.485 μ_B) of three isolated spin-only Fe^{II} ions ($S = 2$, $g = 2.0$; Figure 24b). The $\chi_M T$ value of **2** remains almost constant from 300 to 175 K, and then decreases on further cooling, reaching a value of 4.327 $cm^3 K mol^{-1}$ at 2 K. This behavior indicates a dominant antiferromagnetic interaction between the Fe^{II} ions in the structures. As the shortest Fe···Fe distance across the bpy bridge is 11.370 Å in **2**, the magnetic exchange coupling through the bpy bridge is expected to be very weak.[25] Therefore, the antiferromagnetic interaction between Fe centers is expected to be through the carboxylate bridge. The $1/\chi_M$ versus T plot of **2** is in correspondence with the Curie–Weiss law in the range of 2–300 K with $C = 11.769$ $cm^3 K mol^{-1}$ and $\theta = -3.868$ K.

For **4**, the $\chi_M T$ value at 300 K is 5.654 $cm^3 K mol^{-1}$ (6.725 μ_B), which is much higher than the expected value (3.750 $cm^3 K mol^{-1}$, 5.477 μ_B) of two isolated spin-only Co^{II} ions ($S = 1/2$, $g = 2.0$; Figure 24c). As T is lowered, $\chi_M T$ decreases continuously to a value of 1.019 $cm^3 K mol^{-1}$ at 2 K. This behavior indicates a dominant antiferromagnetic interaction between the Co^{II} ions in the structures. In **4**, the Co···Co distance through the bpy bridge is 11.116 Å, and is 6.652 Å through the bptc bridge. The long Co···Co distances exclude an efficient direct exchange between the Co^{II} ions.[25] Therefore, the overall antiferromagnetic interaction should be mainly attributed to the magnetic exchange coupling within the $[Co_4(CO_2)_4]$ tetranuclear unit. The $1/\chi_M$

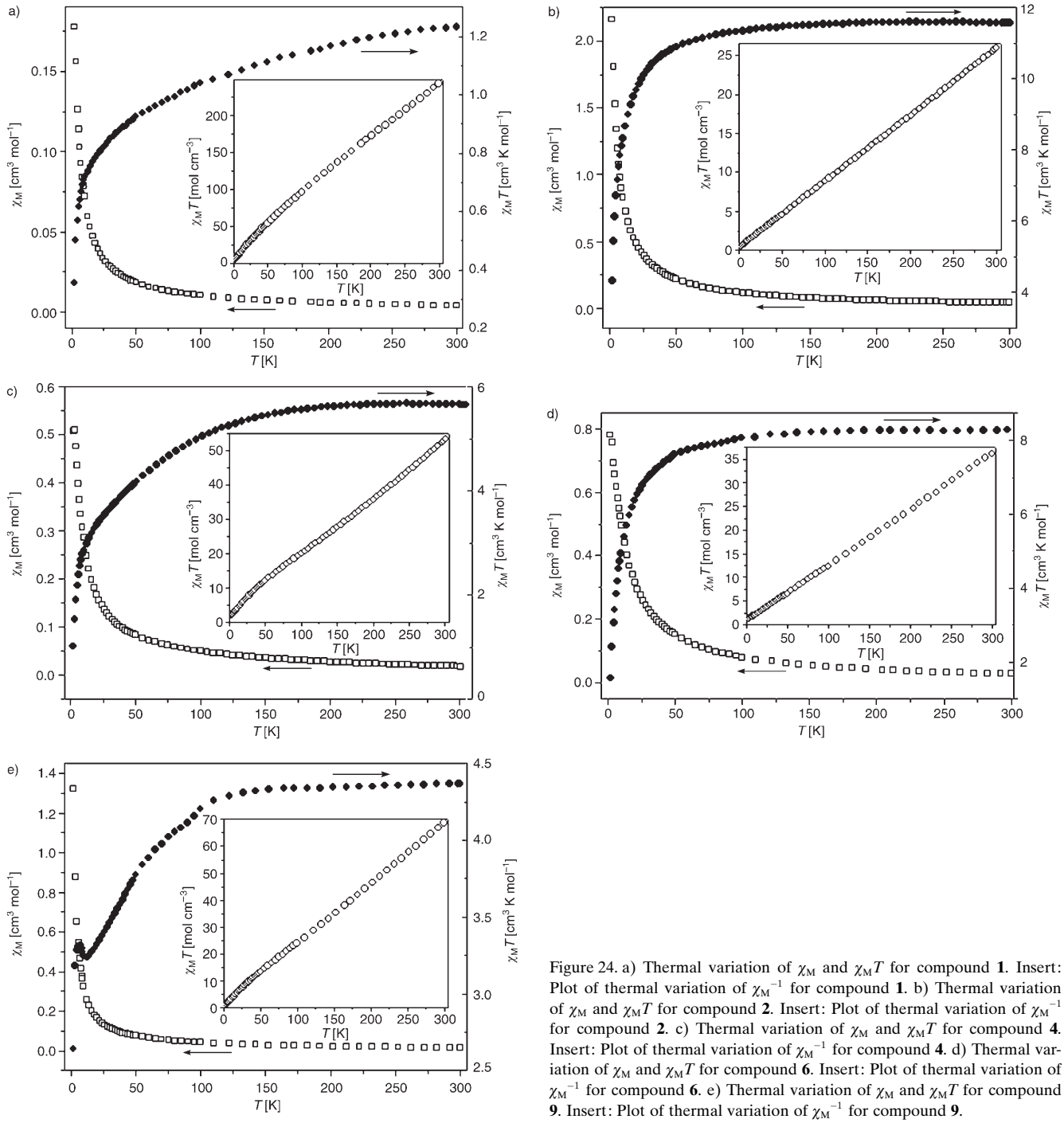

Figure 24. a) Thermal variation of χ_M and $\chi_M T$ for compound **1**. Insert: Plot of thermal variation of χ_M^{-1} for compound **1**. b) Thermal variation of χ_M and $\chi_M T$ for compound **2**. Insert: Plot of thermal variation of χ_M^{-1} for compound **2**. c) Thermal variation of χ_M and $\chi_M T$ for compound **4**. Insert: Plot of thermal variation of χ_M^{-1} for compound **4**. d) Thermal variation of χ_M and $\chi_M T$ for compound **6**. Insert: Plot of thermal variation of χ_M^{-1} for compound **6**. e) Thermal variation of χ_M and $\chi_M T$ for compound **9**. Insert: Plot of thermal variation of χ_M^{-1} for compound **9**.

versus T plot of **4** is in correspondence with the Curie–Weiss law in the range of 18–300 K with $C = 6.018\ \mathrm{cm^3\,K\,mol^{-1}}$ and $\theta = -16.396$ K.

For **6**, the $\chi_M T$ value at 300 K is 8.281 $\mathrm{cm^3\,K\,mol^{-1}}$ (8.139 μ_B), which is slightly smaller than the expected value (8.750 $\mathrm{cm^3\,K\,mol^{-1}}$, 8.367 μ_B) of two isolated spin-only Mn^{II} ions ($S = {}^5/_2$, $g = 2.0$; Figure 24d). The $\chi_M T$ value of **6** remains almost constant from 300 to 162 K, and then decreases on further cooling, reaching a value of 1.560 $\mathrm{cm^3\,K\,mol^{-1}}$ at 2 K. This behavior indicates a dominant antiferromagnetic interaction between the Mn^{II} ions in the structures. In **6**, the Mn···Mn distance through the bpy bridge is 11.727 Å, and is 12.570 Å through the bptc bridge. The long Mn···Mn distances exclude an efficient direct exchange between the Mn^{II} ions.[25] Therefore, the magnetic behavior of **6** can be explained by the magnetic exchange coupling through the carboxylate bridge. The fit of the curve for $1/\chi_M$ versus T plot of **6** to the Curie–Weiss law gives a good result in the temperature range of 2–300 K with $C = 8.501\ \mathrm{cm^3\,K\,mol^{-1}}$ and $\theta = -6.553$ K.

For **9**, the $\chi_M T$ value at 300 K is 4.367 $cm^3 K mol^{-1}$ (5.911 μ_B), which is slightly higher than the expected value (3.750 $cm^3 K mol^{-1}$, 5.477 μ_B) of two isolated spin-only Co^{II} ions ($S = {}^3/_2$, $g = 2.0$; Figure 24e). As T is lowered, $\chi_M T$ continuously decreases and reaches a local minimum of 3.237 $cm^3 K mol^{-1}$ at about 13 K, and then increases to a value 3.319 $cm^3 K mol^{-1}$ at 7 K, before dropping quickly to 2.641 $cm^3 K mol^{-1}$ at 2 K. The magnetic behavior of **9** is unusual and interesting, indicative of a strong antiferromagnetic interaction admixture with a very weak ferromagnetic interaction.[26] The fit of the curve for $1/\chi_M$ versus T plot of **6** to the Curie–Weiss law gives a good result in the temperature range of 5–300 K with $C = 4.467$ $cm^3 K mol^{-1}$ and $\theta = -6.465$ K.

Conclusion

In summary, we have developed a rational synthetic strategy that successfully provided the first pillared helical-layer coordination polymers by appropriate choice of building units for the helical layers and pillars. These pillared helical-layer complexes combined the respective merits of pillared-layer and helical structures. The successful isolation of these solid materials provides not only new types of pillared-layer structures, but also a bridge between pillared-layer and helical systems. The new design idea depicted in this paper may be a promising technique for the construction of many other pillared-layer structures with helical or chiral characters, thus opening a new avenue in the exploration of pillared porous MOFs.

Experimental Section

Materials and physical measurements: All chemicals were commercially purchased and used without further purification. Elemental analyses (C, H and N) were performed on a Perkin-Elmer 2400 CHN Elemental Analyzer. Cu, Fe, Ni, Co, Mn, and Mg were determined by a Leaman inductively coupled plasma (ICP) spectrometer. IR spectra were recorded in the range 400–4000 cm^{-1} on an Alpha Centaurt FT/IR Spectrophotometer using KBr pellets. TG analyses were performed on a Perkin-Elmer TGA7 instrument in flowing N_2 with a heating rate of 10 °C·min^{-1}. Excitation and emission spectra were obtained on a SPEX FL-2T2 spectrofluorometer equipped with a 450 W xenon lamp as the excitation source. Variable-temperature magnetic susceptibility data were obtained on a SQUID magnetometer (Quantum Design, MPMS-7) in the temperature range of 2–300 K with an applied field of 10 KG. XRPD data were recorded on a Siemens D5005 diffractometer using $Cu_{K\alpha}$ radiation.

Preparation

$[Cu_2(bptc)(bpy)_2]$ (1): A mixture of $Cu(OAc)_2{\cdot}H_2O$ (0.5 mmol), H_4bptc (0.25 mmol), bpy (0.5 mmol), and water (7 mL) was stirred for 30 min in air, then transferred and sealed in an 18 mL Teflon-lined autoclave, which was heated at 130 °C for 96 h. After slow cooling to the room temperature, blue block-like crystals of **1** were filtered off, washed with distilled water, and dried at ambient temperature (76% based on Cu). Elemental analysis calcd (%) for $C_{37}H_{22}Cu_2N_4O_9$ (793.67): C 55.99, H 2.79, Cu 16.01, N 7.06; found: C 56.21, H 2.87, Cu 15.96, N 6.95; selected IR (KBr): $\tilde{\nu}$ = 1630 s, 1613 s, 1489 m, 1415 s, 1386 s, 1367 s, 1276 m, 1242 s, 1225 m, 1084 w, 1071 m, 912 w, 850 m, 833 s, 806 m, 765 m, 666 w, 642 m, 515 m cm^{-1}.

$[M_3(Hbptc)_2(bpy)_3(H_2O)_4]{\cdot}2H_2O$ (M = Fe(2) and Ni(3)): A mixture of $FeSO_4{\cdot}7H_2O$ (0.5 mmol), H_4bptc (0.25 mmol), bpy (0.5 mmol), and water (7 mL) was stirred for 30 min in air, then transferred and sealed in an 18 mL Teflon-lined autoclave, which was heated at 130 °C for 96 h. After slow cooling to the room temperature, red block-like crystals of **2** were filtered off, washed with distilled water, and dried at ambient temperature (55% based on Fe). Elemental analysis calcd (%) for $C_{64}H_{50}Fe_3N_6O_{24}$ (1454.65): C 52.84, H 3.46, Fe 11.52, N 5.78; found: C 52.70, H 3.57, Fe 11.29, N 5.91, selected IR (KBr): $\tilde{\nu}$ = 3535 m, 3425 m, 1649 s, 1607 s, 1575 s, 1490 s, 1413 s, 1368 s, 1301 s, 1247 m, 1219 m, 1181 w, 1067 m, 983 w, 896 m, 851 w, 839 m, 815 s, 789 m, 759 m, 721 m, 660 m, 631 m, 614 m cm^{-1}.

The preparation of **3** was similar to that of **2** except that $NiCl_2{\cdot}6H_2O$ was used instead of $FeSO_4{\cdot}7H_2O$. Green block-like crystals were obtained in 47% yield. Elemental analysis calcd (%) for $C_{64}H_{50}N_6Ni_3O_{24}$ (1463.23): C 52.53, H 3.44, N 5.74, Ni 12.03; found: C 52.31, H 3.51, N 5.83, Ni 12.09; selected IR (KBr): $\tilde{\nu}$ = 3526 m, 3390 m, 1650 s, 1607 s, 1572 s, 1490 s, 1416 s, 1368 s, 1302 s, 1248 m, 1219 m, 1181 w, 1078 m, 1068 m, 984 m, 896 m, 850 w, 838 m, 816 s, 788 m, 759 m, 721 s, 659 m, 634 m, 615 m cm^{-1}.

$[Co_2(bptc)(bpy)(H_2O)]{\cdot}0.5bpy$ (4): A mixture of $Co(OAc)_2{\cdot}4H_2O$ (0.5 mmol), H_4bptc (0.25 mmol), bpy (0.5 mmol), and water (7 mL) was stirred and adjusted to pH 9.0 with a 2.5 M NaOH solution, then transferred and sealed in an 18 mL Teflon-lined autoclave, which was heated at 150 °C for 96 h. After slow cooling to the room temperature, purple block-like crystals of **4** were filtered off, washed with distilled water, and dried at ambient temperature (yield: 68% based on Co). Elemental analysis calcd (%) for $C_{32}H_{20}Co_2N_3O_{10}$ (724.37): C 53.06, H 2.78, Co 16.27, N 5.80; found: C 52.95, H 2.86, Co 16.04, N 5.69; selected IR (KBr): $\tilde{\nu}$ = 3362 br, 1670 m, 1612 s, 1597 s, 1567 s, 1492 s, 1413 s, 1363 s, 1300 s, 1244 s, 1220 m, 1082 s, 1070 s, 1046 w, 996 w, 852 s, 804 s, 754 s, 726 s, 673 m, 642 s, 521 s cm^{-1}.

$[Cd_2(bptc)(bpy)(H_2O)_2]{\cdot}H_2O$ (5): A mixture of $Cd(NO_3)_2{\cdot}4H_2O$ (0.5 mmol), H_4bptc (0.25 mmol), bpy (0.5 mmol), and water (7 mL) was stirred and adjusted to pH 9.0 with a 2.5 M NaOH solution, then transferred and sealed in an 18 mL Teflon-lined autoclave, which was heated at 130 °C for 96 h. After slow cooling to the room temperature, colorless platelet crystals of **5** were filtered off, washed with distilled water, and dried at ambient temperature (76% based on Cd). Elemental analysis calcd (%) for $C_{27}H_{20}Cd_2N_2O_{12}$ (789.25): C 41.09, H 2.55, Cd 28.49, N 3.55; found: C 41.21, H 2.62, Cd 28.58, N 3.78; selected IR (KBr): $\tilde{\nu}$ = 3223 brm, 1659 s, 1593 s, 1551 s, 1532 s, 1492 s, 1378 s, 1278 m, 1251 m, 1088 m, 857 s, 813 s, 799 m, 760 s, 710 m, 666 m, 621 m, 485 m cm^{-1}.

$[Mn_2(bptc)(bpy)_{1.5}(H_2O)_3]$ (6): A mixture of $MnCl_2{\cdot}4H_2O$ (0.5 mmol), H_4bptc (0.25 mmol), bpy (0.5 mmol), and water (7 mL) was stirred and adjusted to pH 9.0 with a 2.5 M NaOH solution, then transferred and sealed in an 18 mL Teflon-lined autoclave, which was heated at 150 °C for 96 h. After slow cooling to room temperature, colorless block-like crystals of **6** were filtered off, washed with distilled water, and dried at ambient temperature (84% based on Mn). Interestingly when the above-mentioned reaction was carried out at 110 °C for 72 h and then at 150 °C for another 48 h, compound **6** was also isolated (55%). Elemental analysis calcd (%) for $C_{32}H_{24}Mn_2N_3O_{12}$ (752.42): C 51.08, H 3.21, Mn 14.60, N 5.58; found: C 50.96, H 3.24, Mn 14.48, N 5.81; selected IR (KBr): $\tilde{\nu}$ = 3294 brm, 1658 s, 1576 s, 1484 s, 1407 s, 1352 s, 1302 s, 1273 m, 1236 s, 1085 m, 1064 m, 906 w, 853 s, 812 s, 768 m, 619 s cm^{-1}.

$[M_2(bptc)(bpy)_{0.5}(H_2O)_5]{\cdot}0.5bpy$ [M = Mn(7), Mg(8) and Co(9)]: A mixture of $MnCl_2{\cdot}4H_2O$ (0.5 mmol), H_4bptc (0.25 mmol), bpy (0.5 mmol), and water (7 mL) was stirred and adjusted to pH 9.0 with a 2.5 M NaOH solution, then transferred and sealed in an 18 mL Teflon-lined autoclave, which was heated at 110 °C for 72 h. After slow cooling to room temperature, yellow block-like crystals of **7** were filtered off, washed with distilled water, and dried at ambient temperature (32% based on Mn). Elemental analysis calcd (%) for $C_{27}H_{24}Mn_2N_2O_{14}$ (710.36): C 45.65, H 3.41, Mn 15.47, N 3.94; found: C 45.90, H 3.34, Mn 15.36, N 4.08; selected IR (KBr): $\tilde{\nu}$ = 3422 s, 3281 s, 1649 s, 1606 s, 1489 s, 1448 m, 1410 s, 1302 s, 1280 s, 1240 s, 1088 m, 1066 m, 1007 w, 843 m, 814 s, 721 m, 700 m, 665 m, 473 m cm^{-1}.

Table 1. Crystal data and structure refinement for **1–9**.

	1	**2**	**3**	**4**	**5**	**6**	**7**	**8**	**9**
formula	$C_{37}H_{22}Cu_2N_4O_9$	$C_{64}H_{50}Fe_3N_6O_{24}$	$C_{64}H_{50}Ni_3N_6O_{24}$	$C_{32}H_{20}Co_2N_3O_{10}$	$C_{27}H_{20}Cd_2N_2O_{12}$	$C_{32}H_{24}Mn_2N_3O_{12}$	$C_{27}H_{24}Mn_2N_2O_{14}$	$C_{27}H_{24}Mg_2N_2O_{14}$	$C_{27}H_{24}Co_2N_2O_{14}$
F_w	793.67	1454.65	1463.23	724.37	789.25	752.42	710.36	649.10	718.34
crystal system	orthorhombic	monoclinic	monoclinic	monoclinic	monoclinic	triclinic	triclinic	triclinic	triclinic
space group	*Fdd*2	*P*2/*c*	*P*2/*c*	$P2_1/n$	$P2_1/n$	$P\bar{1}$	$P\bar{1}$	$P\bar{1}$	$P\bar{1}$
a [Å]	23.243(5)	11.370(2)	11.254(2)	10.999(2)	7.1108(14)	10.402(2)	9.965(2)	9.777(2)	9.788(2)
b [Å]	27.437(6)	11.490(2)	11.312(2)	14.993(3)	13.699(3)	11.850(2)	10.819(2)	10.669(2)	10.661(2)
c [Å]	11.451(2)	22.933(5)	22.898(5)	16.700(3)	27.255(6)	13.880(3)	15.607(3)	15.434(3)	15.452(3)
α [°]	90	90	90	90	90	107.41(3)	109.39(3)	109.52(3)	109.26(3)
β [°]	90	93.91(3)	93.29(3)	95.57(3)	94.34(3)	94.88(3)	97.90(3)	97.14(3)	98.00(3)
γ [°]	90	90	90	90	90	111.22(3)	105.99(3)	106.21(3)	105.84(3)
V [Å^3]	7303(3)	2989.3(10)	2910.0(10)	2741.0(10)	2647.3(9)	1485.3(5)	1476.5(5)	1414.2(5)	1416.8(5)
Z	8	2	2	4	4	2	2	2	2
ρ_{calcd} [g cm^{-3}]	1.444	1.616	1.670	1.755	1.980	1.682	1.598	1.524	1.684
μ [mm^{-1}]	1.224	0.812	1.057	1.282	1.679	0.925	0.929	0.163	1.248
R_1 $[I>2\sigma(I)]$[a]	0.0688	0.0563	0.0487	0.0301	0.0357	0.0467	0.0406	0.0487	0.0430
wR_2 (all data)[b]	0.1145	0.1668	0.1305	0.0953	0.0796	0.1491	0.1272	0.1637	0.1375

[a] $R_1 = \Sigma||F_0| - |F_C||/\Sigma|F_0|$. [b] $wR_2 = \Sigma[w(F_o^2 - F_c^2)^2]/\Sigma[w(F_o^2)^2]^{1/2}$.

The preparations of **8** and **9** were similar to that of **7** except that $Mg(NO_3)_2{\cdot}6H_2O$ and $CoCl_2{\cdot}6H_2O$ were used instead of $MnCl_2{\cdot}4H_2O$. Colorless block-like crystals of **8** were obtained (69%). Elemental analysis calcd (%) for $C_{27}H_{24}Mg_2N_2O_{14}$ (649.10): C 49.96, H 3.73, Mg 7.49, N 4.32; found: C 50.13, H 3.80, Mg 7.53, N 4.43; selected IR (KBr): $\tilde{\nu}$ = 3420 s, 3282 s, 1651 s, 1607 s, 1488 s, 1448 m, 1412 s, 1301 s, 1281 s, 1241 s, 1089 m, 1067 m, 1007 w, 843 m, 815 s, 722 m, 700 m, 666 m, 474 m cm^{-1}. Brown block-like crystals of **9** were obtained (56%). Elemental analysis calcd (%) for $C_{27}H_{24}Co_2N_2O_{14}$ (718.34): C 45.15, H 3.37, Co 16.41, N 3.90; found: C 45.27, H 3.44, Co 16.19, N 3.81; selected IR (KBr): $\tilde{\nu}$ = 3421 s, 3283 s, 1650 s, 1601 s, 1487 s, 1448 m, 1411 s, 1380 s, 1300 s, 1283 s, 1242 s, 1089 m, 1068 m, 1007 w, 723 m, 700 m, 665 m, 475 m cm^{-1}.

Crystal structure determination: Intensity data were collected on a Rigaku R-AXIS RAPID IP diffractometer with $Mo_{K\alpha}$ monochromated radiation (λ = 0.71073 Å) at 293 K. Empirical absorption correction was applied. The structures of **1–9** were solved by the direct method and refined by the Full-matrix least squares on F^2 using the SHELXL-97 software.[27] All of the non-hydrogen atoms were refined anisotropically. The organic hydrogen atoms were generated geometrically; the aqua hydrogen atoms were located from difference maps and refined with isotropic temperature factors. A summary of crystal data and structure refinement for compounds **1–9** is provided in Table 1.

CCDC-278613, -285615 to -285622 contain the supplementary crystallographic data for this paper. These data can be obtained free of charge from the Cambridge Crystallographic Data Centre via www.ccdc.cam.ac.uk/data_request/cif.

Acknowledgements

The authors thank the National Natural Science Foundation of China (20371011) for financial support.

[1] a) A. K. Cheetham, G. Férey, T. Loiseau, *Angew. Chem.* **1999**, *111*, 3466; *Angew. Chem. Int. Ed.* **1999**, *38*, 3268; b) K. Biradha, Y. Hongo, M. Fujita, *Angew. Chem.* **2000**, *112*, 4001; *Angew. Chem. Int. Ed.* **2000**, *39*, 3843; c) M. C. Hong, Y. J. Zhao, W. P. Su, R. Cao, M. Fujita, Z. Y. Zhou, A. S. C. Chan, *Angew. Chem.* **2000**, *112*, 2586; *Angew. Chem. Int. Ed.* **2000**, *39*, 2468; d) F. Schüth, W. Schmidt, *Adv. Mater.* **2002**, *14*, 629; e) K. Campbell, C. J. Kuehl, M. J. Ferguson, P. J. Stang, R. R. Tykwinski, *J. Am. Chem. Soc.* **2002**, *124*, 7266.

[2] a) H. Li, M. Eddaoudi, M. O'Keeffe, O. M. Yaghi, *Nature* **1999**, *402*, 276; b) B. Chen, M. Eddaoudi, S. T. Hyde, M. O'Keeffe, O. M. Yaghi, *Science* **2001**, *291*, 1021; c) J. Kim, B. Chen, T. M. Reineke, H. Li, M. Eddaoudi, D. B. Moler, M. O'Keeffe, O. M. Yaghi, *J. Am. Chem. Soc.* **2001**, *123*, 8239; d) N. L. Rosi, M. Eddaoudi, J. Kim, M. O'Keeffe, O. M. Yaghi, *Angew. Chem.* **2002**, *114*, 294; *Angew. Chem. Int. Ed.* **2002**, *41*, 284; e) M. Eddaoudi, J. Kim, N. Rosi, D. Vodak, D. V. Wachter, M. O'Keeffe, O. M. Yaghi, *Science* **2002**, *295*, 469; f) N. L. Rosi, J. Eckert, M. Eddaoudi, D. T. Vodak, J. Kim, M. O'Keeffe, O. M. Yaghi, *Science* **2003**, *300*, 1127.

[3] a) B. F. Abrahams, M. Moylan, S. D. Orchard, R. Robson, *Angew. Chem.* **2003**, *115*, 1892; *Angew. Chem. Int. Ed.* **2003**, *42*, 1848; b) C. Qin, X. L. Wang, L. Carlucci, M. L. Tong, E. B. Wang, C. W. Hu, L. Xu, *Chem. Commun.* **2004**, 1876; c) C. Y. Su, A. M. Goforth, M. D. Smith, P. J. Pellechia, H. C. zur Loye, *J. Am. Chem. Soc.* **2004**, *126*, 3576; d) D. R. Xiao, Y. G. Li, E. B. Wang, S. T. Wang, Y. Hou, G. J. H. De, C. W. Hu, *Inorg. Chem.* **2003**, *42*, 7652; e) A. Stein, *Adv. Mater.* **2003**, *15*, 763.

[4] a) S. R. Batten, R. Robson, *Angew. Chem.* **1998**, *110*, 1558; *Angew. Chem. Int. Ed.* **1998**, *37*, 1460; b) P. J. Hagrman, D. Hagrman, J. Zubieta, *Angew. Chem.* **1999**, *111*, 2798; *Angew. Chem. Int. Ed.* **1999**, *38*, 2638; c) A. J. Blake, N. R. Champness, P. Hubberstey, W. S. Li, M. A. Withersby, M. Schröder, *Coord. Chem. Rev.* **1999**, *183*, 117; d) J.-P. Zhang, Y.-Y. Lin, X.-C. Huang, X.-M. Chen, *J. Am. Chem. Soc.* **2005**, *127*, 5495; e) M.-L. Tong, X.-M. Chen, S. R. Batten, *J. Am. Chem. Soc.* **2003**, *125*, 16170.

[5] a) O. R. Evans, W. Lin, *Acc. Chem. Res.* **2002**, *35*, 511; b) X. C. Huang, J. P. Zhang, X. M. Chen, *J. Am. Chem. Soc.* **2004**, *126*, 13218; c) J. Zhang, Z.-J. Li, Y. Kang, J.-K. Cheng, Y.-G. Yao, *Inorg. Chem.* **2004**, *43*, 8085; d) L. Carlucci, G. Ciani, D. M. Proserpio, *Coord. Chem. Rev.* **2003**, *246*, 247; e) X.-H. Bu, W. Chen, S.-L. Lu, R.-H. Zhang, D.-Z. Liao, W.-M. Bu, M. Shionoya, F. Brisse, J. Ribas, *Angew. Chem.* **2001**, *113*, 3301; *Angew. Chem. Int. Ed.* **2001**, *40*, 3201.

[6] a) A. Müller, S. K. Das, S. Talismanov, S. Roy, E. Beckmann, H. Bögge, M. Schmidtmann, A. Merca, A. Berkle, L. Allouche, Y. Zhou, L. Zhang, *Angew. Chem.* **2003**, *115*, 5193; *Angew. Chem. Int. Ed.* **2003**, *42*, 5039; b) C. D. Wu, C. Z. Lu, H. H. Zhuang, J. S. Huang, *J. Am. Chem. Soc.* **2002**, *124*, 3836; c) D. N. Dybtsev, H. Chun, K. Kim, *Angew. Chem.* **2004**, *116*, 5143; *Angew. Chem. Int. Ed.* **2004**, *43*, 5033; d) Y. Y. Niu, H. G. Zheng, H. W. Hou, X. Q. Xin, *Coord. Chem. Rev.* **2004**, *248*, 169; e) X. H. Bu, M. L. Tong, H. C. Chang, S. Kitagawa, S. R. Batten, *Angew. Chem.* **2004**, *116*, 194; *Angew. Chem. Int. Ed.* **2004**, *43*, 192.

[7] a) O. M. Yaghi, M. O'Keeffe, N. W. Ockwig, H. K. Chae, M. Eddaoudi, J. Kim, *Nature* **2003**, *423*, 705; b) N. W. Ockwig, O. Delgado-Friederichs, M. O'Keeffee, O. M. Yaghi, *Acc. Chem. Res.* **2005**, *38*, 176; c) S. Kitagawa, R. Kitaura, S. I. Noro, *Angew. Chem.* **2004**, *116*,

2388; *Angew. Chem. Int. Ed.* **2004**, *43*, 2334; d) C. N. R. Rao, S. Natarajan, R. Vaidhyanathan, *Angew. Chem.* **2004**, *116*, 1490; *Angew. Chem. Int. Ed.* **2004**, *43*, 1466; e) B. H. Ye, M. L. Tong, X. M. Chen, *Coord. Chem. Rev.* **2005**, *249*, 545.

[8] a) *Pillared Layered Structures: Current Trends and Applications* (Ed.: I. V. Mitchell), Elsevier, London, **1990**; b) S. Kitagawa, R. Kitaura, *Comments Inorg. Chem.* **2002**, *23*, 106.

[9] a) K. T. Holman, A. M. Pivowar, J. V. Swift, M. D. Ward, *Acc. Chem. Res.* **2001**, *34*, 107; b) M. J. Zaworotko, *Chem. Commun.* **2001**, 1.

[10] a) S. P. Newman, W. Jones, *New J. Chem.* **1998**, *22*, 105; b) T. J. Pinnavaia, *Science* **1983**, *220*, 365; c) G. K. H. Shimizu, G. D. Enright, C. I. Ratcliffe, J. A. Ripmeester, *Chem. Commun.* **1999**, 461.

[11] a) A. Clearfield, *Prog. Inorg. Chem.* **1998**, *47*, 371; b) G. Alberti in *Comprehensive Supramolecular Chemistry, Vol. 7* (Eds.: J. L. Atwood, J. E. Davies, D. D. MacNicol, F. Vögtle), Elsevier, New York, **1996**, p. 151; c) D. Medoukali, P. H. Muti, A. Vioux, *J. Mater. Chem.* **1999**, *9*, 2553.

[12] a) V. A. Russell, C. C. Evans, W. Li, M. D. Ward, *Science* **1997**, *276*, 575; b) M. Kondo, T. Okubo, A. Asami, S. I. Noro, T. Yoshitomi, S. Kitagawa, T. Ishii, H. Matsuzaka, K. Seki, *Angew. Chem.* **1999**, *111*, 190; *Angew. Chem. Int. Ed.* **1999**, *38*, 140; c) Y. Diskin-Posner, S. Dahal, I. Goldberg, *Angew. Chem.* **2000**, *112*, 1344; *Angew. Chem. Int. Ed.* **2000**, *39*, 1288; d) A. P. Côté, G. K. H. Shimizu, *Chem. Commun.* **2001**, 251; e) R. Kitaura, K. Fujimoto, S. Noro, M. Kondo, S. Kitagawa, *Angew. Chem.* **2002**, *114*, 141; *Angew. Chem. Int. Ed.* **2002**, *41*, 133; f) H. L. Ngo, W. Lin, *J. Am. Chem. Soc.* **2002**, *124*, 14298; g) T. J. Prior, D. Bradshaw, S. J. Teat, M. J. Rosseinsky, *Chem. Commun.* **2003**, 500; h) J. L. Song, H. H. Zhao, J. G. Mao, K. R. Dunbar, *Chem. Mater.* **2004**, *16*, 1884.

[13] a) B. Moulton, M. J. Zaworotko, *Chem. Rev.* **2001**, *101*, 1629; b) M. Albrecht, *Chem. Rev.* **2001**, *101*, 3457; c) T. Nakano, Y. Okamoto, *Chem. Rev.* **2001**, *101*, 4013; d) V. Soghomonian, Q. Chen, R. C. Haushalter, J. Zubieta, C. J. O'Connor, *Science* **1993**, *259*, 1596; e) Z. Shi, S. H. Feng, S. Gao, L. Zhang, G. Yang, J. Hua, *Angew. Chem.* **2000**, *112*, 2415; *Angew. Chem. Int. Ed.* **2000**, *39*, 2325.

[14] a) T. E. Gier, X. Bu, P. Feng, G. D. Stucky, *Nature* **1998**, *395*, 154; b) S. Neeraj, S. Natarajan, C. N. R. Rao, *Chem. Commun.* **1999**, 165; c) D. Kumaran, S. Eswaramoorthy, F. W. Studier, S. Swaminathan, *Protein Sci.* **2005**, *14*, 719; d) D. R. Xiao, Y. Xu, Y. Hou, E. B. Wang, S. T. Wang, Y. G. Li, L. Xu, C. W. Hu, *Eur. J. Inorg. Chem.* **2004**, 1385; e) X. L. Wang, C. Qin, E. B. Wang, Y. G. Li, C. W. Hu, L. Xu, *Chem. Commun.* **2004**, 378.

[15] a) X. M. Chen, G. F. Liu. *Chem. Eur. J.* **2002**, *8*, 4811; b) Y. Cui, S. J. Lee, W. Lin, *J. Am. Chem. Soc.* **2003**, *125*, 6014; c) J.-P. Zhang, Y.-Y. Lin, X.-C. Huang, X.-M. Chen, *Chem. Commun.* **2005**, 1258; d) X. L. Wang, C. Qin, E. B. Wang, L. Xu, Z. M. Su, C. W. Hu, *Angew. Chem.* **2004**, *116*, 5146; *Angew. Chem. Int. Ed.* **2004**, *43*, 5036; e) C.-D. Wu, C-Z. Lu, X. Lin, D. -M, Wu, S.-F. Lu, H.-H. Zhuang, J.-S. Huang, *Chem. Commun.* **2003**, 1284; f) O. Mamula, A. v. Zelewsky, T. Bark, G. Bernardinelli, *Angew. Chem.* **1999**, *111*, 3129; *Angew. Chem. Int. Ed.* **1999**, *38*, 2945.

[16] a) M. Kondo, M. Miyazawa, Y. Irie, R. Shinagawa, T. Horiba, A. Nakamura, T. Naito, K. Maeda, S. Utsuno, F. Uchida, *Chem. Commun.* **2002**, 2156; b) D. F. Sun, R. Cao, Y. Q. Sun, W. H. Bi, X. Li, M. C. Hong, Y. J. Zhao, *Eur. J. Inorg. Chem.* **2003**, 38.

[17] a) L. Han, M. C. Hong, R. H. Wang, J. H. Luo, Z. Z. Lin, D. Q. Yuan, *Chem. Commun.* **2003**, 2580; b) J. Liang, Y. Wang, J. H. Yu, Y. Li, R. R. Xu, *Chem. Commun.* **2003**, 882.

[18] a) L. Pan, B. S. Finkel, X. Y. Huang, J. Li, *Chem. Commun.* **2001**, 105; b) L. Pan, X. Y. Huang, J. Li, Y. G. Wu, N. W. Zheng, *Angew. Chem.* **2000**, *112*, 537; *Angew. Chem. Int. Ed.* **2000**, *39*, 527; c) O. R. Evans, W. Lin, *Inorg. Chem.* **2000**, *39*, 2189.

[19] D. R. Xiao, E. B. Wang, H. Y. An, Z. M. Su, Y. G. Li, L. Gao, C. Y. Sun, L. Xu, *Chem. Eur. J.* **2005**, *11*, 6673.

[20] H.-K. Fun, S. S. Sundara Raj, R.-G. Xiong, J.-L. Zuo, Z. Yu, X.-Z. You, *J. Chem. Soc. Dalton Trans.* **1999**, 1915.

[21] a) S. L. James, *Chem. Soc. Rev.* **2003**, *32*, 276; b) M.-L. Tong, S. Kitagawa, H.-C. Chang, M. Ohba, *Chem. Commun.* **2004**, 418; c) M. I. Khan, S. Cevik, R. J. Doedens, *Chem. Commun.* **2001**, 1930; d) L. Pan, T. Frydel, M. B. Sander, X. Y. Huang, J. Li, *Inorg. Chem.* **2001**, *40*, 1271.

[22] a) D. N. Dybtsev, H. Chun, S. H. Yoon, D. Kim, K. Kim, *J. Am. Chem. Soc.* **2004**, *126*, 32; b) R.-G. Xiong, X.-Z. You, B. F. Abrahams, Z. L. Xue, C.-M. Che, *Angew. Chem.* **2001**, *113*, 4554; *Angew. Chem. Int. Ed.* **2001**, *40*, 4422.

[23] a) X.-L. Wang, C. Qin, E.-B. Wang, Z.-M. Su, L. Xu, S. R. Batten, *Chem. Commun.* **2005**, 4789; b) X.-L. Wang, C. Qin, E.-B. Wang, Y.-G. Li, Z.-M. Su, L. Xu, L. Carlucci, *Angew. Chem.* **2005**, *117*, 5974; *Angew. Chem. Int. Ed.* **2005**, *44*, 5824.

[24] a) S. O. H. Gutschke, D. J. Price, A. K. Powell, P. T. Wood, *Angew. Chem.* **2001**, *113*, 1974; *Angew. Chem. Int. Ed.* **2001**, *40*, 1920; b) R. K. Chiang, N. T. Chuang, C. S. Wur, M. F. Chong, C. R. Lin, *J. Solid State Chem.* **2002**, *166*, 158.

[25] L.-M. Zheng, X. Q. Wang, Y. S. Wang, A. J. Jacobson, *J. Mater. Chem.* **2001**, *11*, 1100.

[26] a) J. Tao, Y. Zhang, M.-L. Tong, X.-M. Chen, T. Yuen, C. L. Lin, X. Y. Huang, J. Li, *Chem. Commun.* **2002**, 1342; b) H.-J. Chen, Z.-W. Mao, S. Gao, X.-M. Chen, *Chem. Commun.* **2001**, 2320; c) C.-M. Liu, S. Gao, H.-M. Hu, X. L. Jin, H.-Z. Kou, *J. Chem. Soc. Dalton Trans.* **2002**, 598.

[27] a) G. M. Sheldrick, SHELXS 97, Program for Crystal Structure Solution, University of Göttingen (Germany), **1997**; b) G. M. Sheldrick, SHELXL 97, Program for Crystal Structure Refinement, University of Göttingen (Germany), **1997**.

Received: October 21, 2005
Revised: February 17, 2006
Published online: June 14, 2006

